(Received 15 December 2023, Accepted 28 February 2024, Scheduled 4 March 2024)

Radio-Frequency Energy Harvester for a Hybrid Power Supply with Constant Voltage Output to a Water Meter

Junlin Mi, Ruinan Fan, Jianwei Jing, Liping Yan, and Changjun Liu*

School of Electronics and Information Engineering, Sichuan University, Chengdu 610064, China

ABSTRACT: This manuscript proposes a hybrid energy harvest and management system to manage harvested ambient thermal and radio frequency (RF) energy and provide constant voltage for an electronic water meter. It mainly includes an antenna, a rectifier, thermoelectric generators (TEGs), and an energy management circuit. The antenna harvests the ambient RF power, and the rectifier converts it to DC power. The harvested RF and thermal powers are stored in a capacitor and managed by an FEH710 energy management circuit to power an electronic water meter. Eight thermoelectric generators convert thermal energy into DC power. The proposed hybrid energy harvesting and management system has been evaluated by simulation and measurement. The antenna's reflection coefficient and peak gain at 2.45 GHz are −30 dB and 3.6 dBi, respectively. The rectifier's measured RF-DC power conversion efficiency (PCE) is 66.7% at 0 dBm. As a demonstration, a commercial electronic water meter works stably by the harvested ambient RF and thermal energy. The proposed hybrid energy harvesting system is expected to find potential practical applications for the Internet of Things (IoT) in environments with RF radiation coverage and temperature gradients.

1. INTRODUCTION

In recent years, with the increasing popularity of Wireless Sensor Networks (WSN) and IoT, low-power electronic devices have been widely used. It is difficult to maintain and replace batteries for a large number of low-power devices. Harvesting technologies of environmental energy, such as solar, thermal, wind, and RF energy [1–4], may become a valuable solution for the power supply to low-power electronic devices. RF energy, as one of the environmental energy sources, has been extensively studied in the context of energy harvesting due to its ubiquity in radio broadcasts, base stations, and Wi-Fi signals [5–14]. A thermoelectric generator (TEG) is a solid-state component that directly converts thermal energy into electricity and is also attracting attention as an independent, clean, renewable energy source. Its conversion efficiency is relatively high [15–17]. A hybrid power harvester containing a solar cell and rectenna was proposed in [18]. When the RF power level is −20 dBm, the RF-DC PCE is about 15%. In [19], a highly integrated hybrid energy harvester was developed for harvesting solar, artificial light, thermal, and RF energy, focusing on designing topologies to achieve high circuit integration and large output power. A thermal source has been used as a bias for diodes to change the diode operating point in hybrid energy harvesters, resulting in increased RF-DC PCE for hybrid energy harvesting [20, 21]. To harvest the thermal energy and RF energy, a triple-band heatsink antenna is proposed, which serves as a part of a triple-band RF energy harvester and also acts as a heatsink that boosts the performance of the thermal energy harvester [22, 23]. However, the output voltage with these strategies is unstable, and it is difficult to drive the load in practice.

This manuscript proposes a circuit for ambient thermal and RF energy harvesting, including an antenna, a rectifier circuit, an energy management circuit, and thermoelectric generators (TEGs). Eight thermoelectric generators are attached to a smart water meter's metal pipe to convert thermal energy into electrical energy. The antenna and rectifier circuit operate in the WiFi band to absorb ambient RF energy. The energy from the rectifier and TEG is stored and managed by an FEH710 energy management circuit to provide constant voltage for the smart water meter.

This manuscript is arranged as follows. Section 2 shows the antenna design and measured results. Section 3 shows the rectifier design and measurements. Section 4 shows the rectenna measurement setup and output DC power. Section 5 explains the mechanism of the energy management circuit and measures its power consumption. Section 6 concludes this manuscript.

2. ANTENNA DESIGN AND FABRICATION

The geometry and fabrication of the proposed antenna are shown in Figure 1. It is an enhanced monopole antenna with an F4B substrate ($\varepsilon_r = 2.65$, $\tan\delta = 0.02$) at a thickness of 1 mm. The top and bottom layers use 18 µm thick copper as the patches. The dimension of the antenna is $60 \times 55 \times 1\,\text{mm}^3$. A rectangular ring slot is etched on the ground plane to realize broadband performance, shifting the antenna's capacitance and inductance to achieve better impedance matching and radiation efficiency [24].

The antenna is simulated and optimized by the ANSYS High Frequency Structure Simulator (HFSS) and measured by a vector network analyzer (Agilent N5230A). A comparison between the simulated and measured voltage reflection coefficients $|S_{11}|$

* Corresponding author: Changjun Liu (cjliu@ieee.org,cjliu@scu.edu.cn).

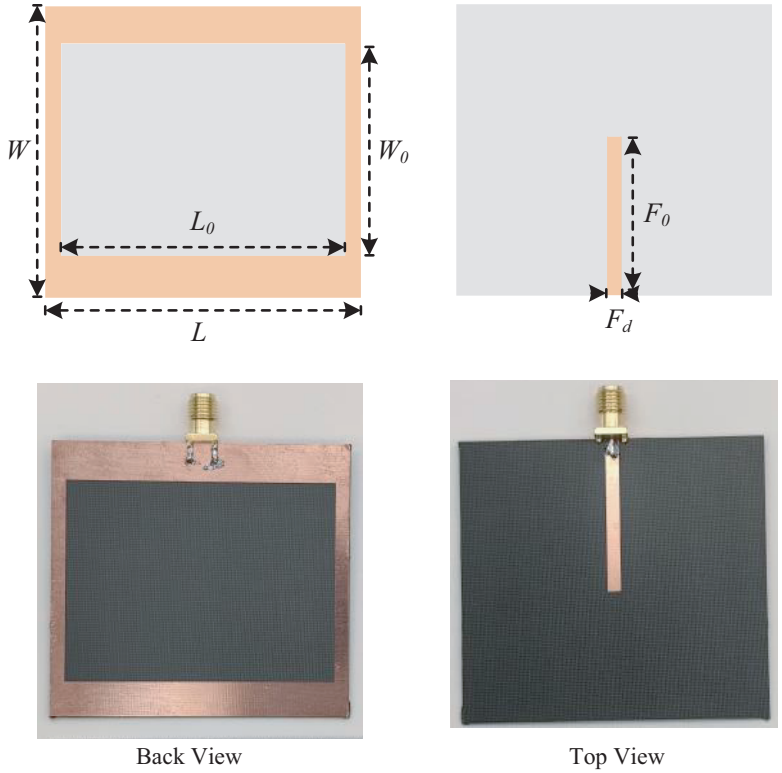

FIGURE 1. Geometry and fabrication of the proposed broadband antenna: $L = 60\,\text{mm}$, $L_0 = 54\,\text{mm}$, $W_0 = 40\,\text{mm}$, $W = 55\,\text{mm}$, $F_d = 2.69\,\text{mm}$, and $F_0 = 30\,\text{mm}$.

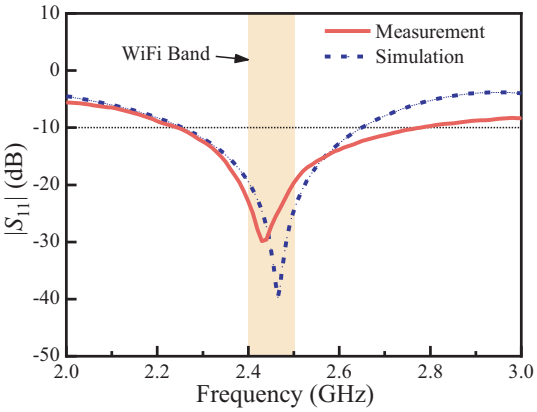

FIGURE 2. Simulated and measured $|S_{11}|$.

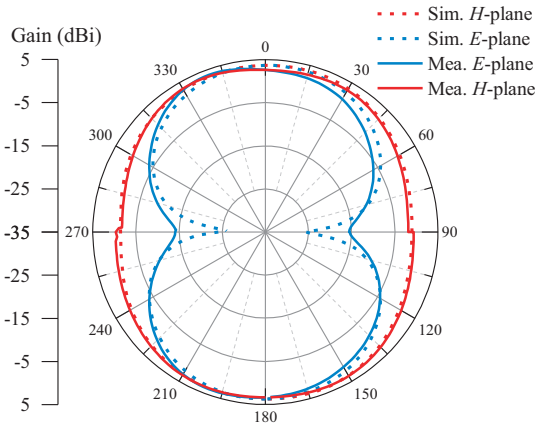

FIGURE 3. Measured and simulated radiation patterns.

is illustrated in Figure 2. It can be seen that the measured results show an excellent agreement with the simulated one. The operating bands range from 2.25 to 2.75 GHz. The $|S_{11}|$ in the WiFi band is below $-20\,\text{dB}$.

The antenna's simulated and measured radiation patterns have consistency in the E-plane (yz-plane) and H-plane (xz-plane), as shown in Figure 3. An omnidirectional radiation characteristic is displayed in the H-plane, and a bi-direction radiation pattern is shown in the E-plane with two opposite directions of $+z$ and $-z$ directions. The peak realized gain is 3.7 dBi. In the area of RF energy harvesting, an antenna with broad beamwidth is ideal. The proposed antenna has an omnidirectional radiation performance to harvest ambient WiFi power.

3. RECTIFIER DESIGN

In ambient RF energy harvesting, the harvested RF power is usually low. A Schottky diode SMS-7630 is selected to design a rectifier circuit with high RF-DC PCE at low input power. The main SPICE parameters of the SMS-7630 diode are listed in Table 1. The junction capacitance is as low as 0.14 pF, and the forward voltage drop is only 0.34 V. Therefore, the SMS-7630 diode obtains high RF-DC PCE in a low RF power environment.

A microwave rectifier circuit generally comprises an input filter, a rectifying diode, an output low-pass filter, a DC load, and an impedance-matching circuit. The schematic of the proposed microwave rectifier is shown in Figure 4.

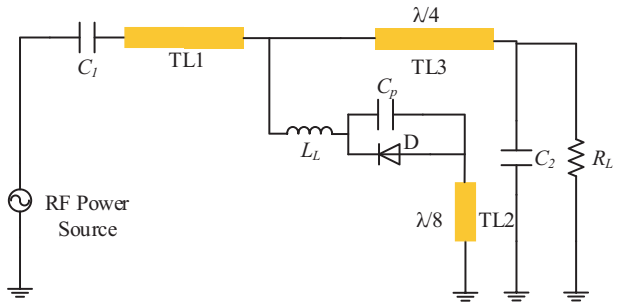

FIGURE 4. Schematic of the microwave rectifier.

B_V	C_{J0}	I_S	R_S	V_{bi}
2 V	0.14 pF	5×1^{-6} A	20 Ω	0.34 V

TABLE 1. Spice parameter of an SMS-7630 diode.

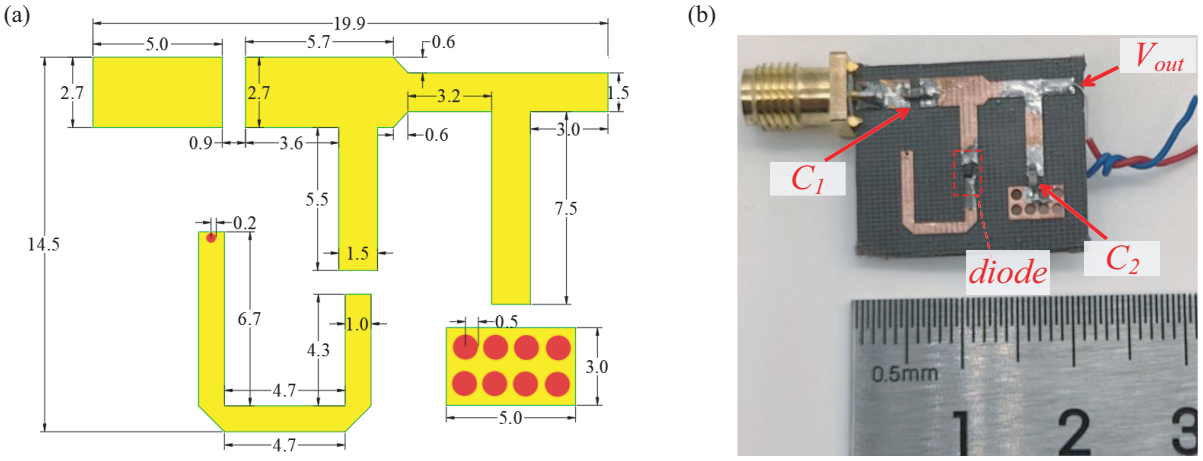

FIGURE 5. (a) Layout of the design. (b) Fabricated rectifier.

The series inductor (L_L) of 1 nH and the shunt capacitor (C_p) of 0.1 pF are equivalent circuit elements of the Schottky diode SC-79 package. The microwave source provides RF power to the rectifier circuit through DC block C_1. A Schottky diode typically presents capacitive impedance due to its internal Schottky junction structure. To facilitate the impedance-matching circuit of the rectifier, it is essential to compensate for the diode capacitive impedance. A short-ended microstrip line compensates for the diode capacitive impedance [25]. The impedance of a short-ended eighth-wavelength microstrip line is

$$Z_{IN} = jZ_0 \tan\left(\frac{\pi}{4}\frac{\omega}{\omega_0}\right) = \begin{cases} 0, & \omega = 0 \\ jZ_0, & \omega = \omega_0 \\ \infty, & \omega = 2\omega_0 \end{cases} \quad (1)$$

where Z_0 is the characteristic impedance of the short-ended microstrip transmission line, and ω_0 is the fundamental frequency.

TL1 matches the impedance of the rectifier circuit to the impedance of the RF power source. The short-ended transmission line TL2 presents a short circuit to pass through the DC power, providing a path for the DC power output. The transmission line TL2 is bent to reduce the area of the rectifier circuit. The short-ended microstrip transmission line at the fundamental frequency presents an inductive impedance to compensate for the diode capacitive impedance. It turns into an open circuit to block the second harmonic produced during rectifying for energy recycling. By adjusting the characteristic impedance Z_0 of the transmission line, its equivalent inductive impedance is tuned. The capacitor C_2 and $\lambda/4$ transmission line TL3 form an output low-pass filter.

The rectifying circuit is designed and optimized by the harmonic balance simulator in the advanced design system (ADS) to achieve high RF-DC PCE. The capacitors C_1 and C_2 are 6.8 and 10 pF, respectively, obtained from the ADS optimization. The final layout of the proposed microwave rectifier and the photo of the fabricated rectifier are shown in Figures 5(a) and (b), respectively. The substrate is F4B with size 19.9 mm × 14.5 mm.

An Agilent E8267C is the signal source, and a standard resistance box is the output DC load. The RF-DC PCE of the rectifier is defined as

$$\eta = \frac{P_{out}}{P_{in}} = \frac{V_{out}^2}{P_{in} \times R_L} \times 100\% \quad (2)$$

where P_{out} is the DC output power, P_{in} the available power from the microwave source, V_{out} the output voltage, and R_L the DC load.

When the input power of the source is 0 dBm at 2.45 GHz, Figure 6 shows the simulated and measured efficiencies with various DC load impedances. The calculated results show an excellent agreement with the simulated one. When the load impedance ranges from 1.2 kΩ to 3 kΩ, the efficiency is greater than 60%. The efficiency is 45% at 500 Ω, and the peak efficiency is 66% at 2.2 kΩ. When R_L is 2.2 kΩ, the input power

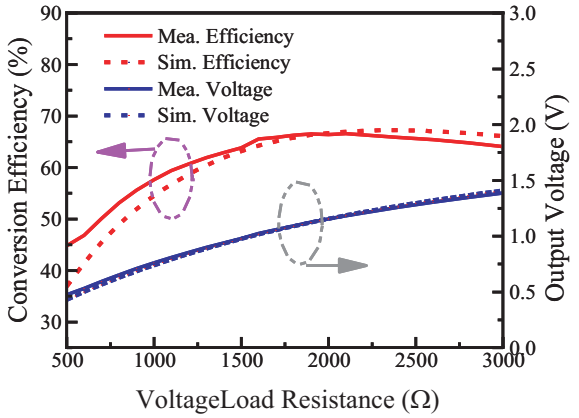

FIGURE 6. Measured and simulated RF-DC conversion efficiency versus load resistance with the input power of 0 dBm at 2.45 GHz.

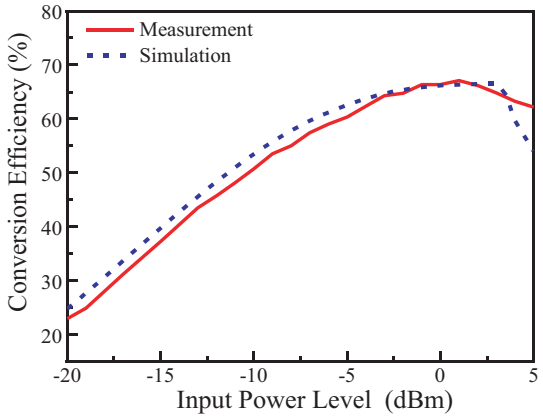

FIGURE 7. Measured and simulated RF-DC conversion efficiency versus input power with R_L of 2.2 kΩ at 2.45 GHz.

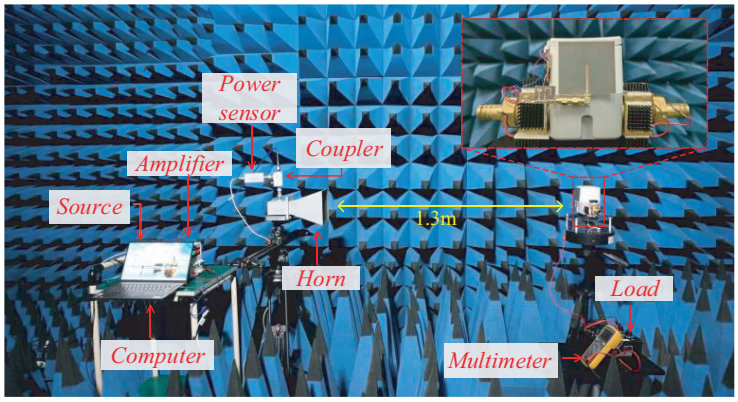

FIGURE 8. Rectenna measurement setup.

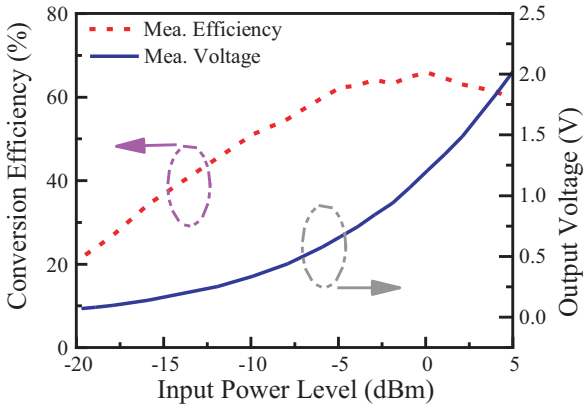

FIGURE 9. Measured conversion efficiency of the rectenna.

is changed from −20 dBm to 5 dBm to obtain the simulated and measured efficiencies at 2.45 GHz. The specific results are shown in Figure 7. The measured results are consistent with the simulation ones. The efficiency increases with the input power increase and reaches a maximum of 66% at 0 dBm and 22% at −20 dBm.

4. RECTENNA MEASUREMENT

A rectenna test system with application to the smart water meter is shown in Figure 8. The system is placed in a microwave anechoic chamber. The computer is used to control the microwave source, and the multimeter is used to test the efficiency which is necessary in this test system. The power from the microwave power source is amplified by an amplifier. A directional coupler is connected to a Mini-Circuits PWR-8GHS power meter to monitor the transmitting power. The gain G_t of the horn antenna is 12.96 dB. The distance between the transmitting antenna and the rectenna is 1.3 m, which is in the far field of the transmitting antenna. The rectenna is on the surface of the water meter case. A standard resistance box is used as the DC load with a multimeter to measure the output voltage.

The efficiency of the rectenna is defined as

$$\eta = \frac{P_{dc}}{P_r} \times 100\% = \frac{V_{dc}^2}{P_r \times R_L} \times 100\% \tag{3}$$

where P_{dc} is the DC output power at load R_L, P_r the received power of the rectenna, V_{dc} the output voltage, and R_L ithe DC load. The received power P_r is calculated by the Friis transmission equation

$$P_r = P_t \left(\frac{\lambda_0}{4\pi R}\right)^2 G_r G_t \tag{4}$$

where P_t and G_t are the power and antenna gain of the transmitting antenna; G_r is the antenna gain of the receiving antenna; and R is the distance between the transmitting and receiving antennas.

The measured RF-DC conversion efficiency of the proposed rectenna is shown in Figure 9. The RF-DC conversion efficiency reaches a maximum of 65% at 0 dBm. The performance comparison between the proposed rectenna and related designs is depicted in Table 2. It is seen from the results that the rectenna has a high conversion efficiency in the application of low-power RF energy harvesting, which provides DC power to subsequent energy management circuits.

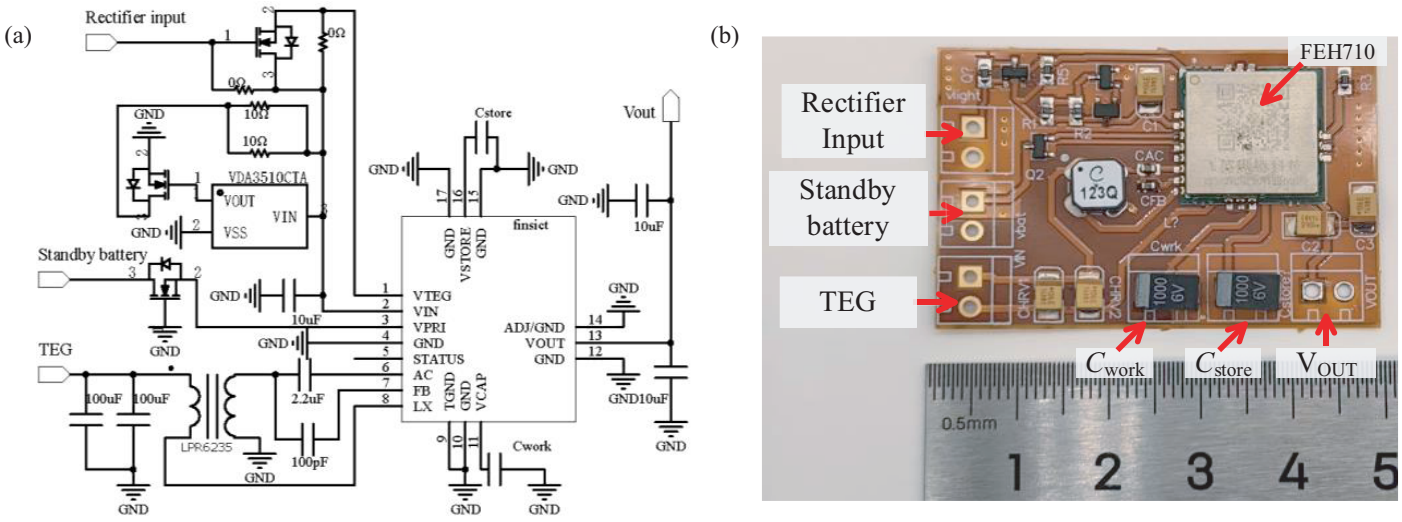

FIGURE 10. Energy management circuit. (a) Schematic diagram. (b) Fabricated energy management circuit.

TABLE 2. Comparison of the proposed rectenna and related designs.

References	Frequency (GHz)	Dimensions (mm)	Single element or array	Input power	Efficiency
[28]	2.45	Single element: $20 \times 10 \times 1$	1	0, −20	Rectifier: 60%, 18%
[27]	1.7–1.8, 2.1–2.7	Array: $145 \times 145 \times 1.53$	1×12	−3, −20	System: 66%, 22%
[29]	2.45	Array: $240 \times 180 \times 1.5$	$3 \times 2 \times 3$	0	Rectenna: 52%
This work	2.45	Single element: $20 \times 15 \times 1$	1	0, −20	Rectenna: 65%, 20%

5. ENERGY MANAGEMENT CIRCUIT

Thermal power is harvested through a TEG device TEC-12701 based on the Seebeck effect [26], which is capable of generating a DC voltage using a temperature gradient between two different semiconductors. The energy from the rectifier and the TEG is stored in a capacitor C_{work} and then managed by a FEH710 energy management circuit which is developed by FINSIOT and outputs a constant voltage of 3.3 V. When the capacitor's energy is sufficient, the built-in switch turns on, and the circuit begins to power the load. If there is extra energy besides consumed energy at the load, the excess energy is stored in the capacitor C_{store}. If the power from the rectifier and the TEG is insufficient, the capacitor C_{store} or standby battery supplies energy to the load. The substrate of the energy management circuit is made of flexible polyimide.

The specific circuit diagrams are shown in Figure 10. Eight semiconductor plates TEC-12701 as the TEGs are attached to the surface of the water pipe to convert thermal energy into electrical energy. Cooling fins are attached to the back of the TEC-12701 to increase their working efficiency. We connect eight semiconductor plates' output ports in series to the FEH710 energy management circuit. The rectenna attached to the water meter collects RF energy as well. The overall system is shown in Figure 11(a), and the system block diagram is shown in Figure 11(b). The experimental results in Figure 12 explain the working mechanism of the energy management circuit. It shows the power consumption of the device driven by rectennas and TEGs. A low-power analyzer LPT2020 is used for power testing at the ambient temperature of 20°C and water temperature of 9°C. The operating voltage of the load is 3.3 V, and the average power consumption is 36.3 µW. The voltage of the standby battery is 3.3 V.

When the water flows, the temperature difference between the water pipe and air is about 11°C, and the voltage of C_{work} starts to rise due to the power generated from the TEGs. Initially, there is no output, and the battery has only 1 µA leakage current. After the voltage of C_{work} reaches 3.1 V, the electronic water meter starts to operate, and the battery current is still at a leakage current of 1 µA. At this time, the power consumption of the standby battery is only 3.3 µW, and the water meter is driven entirely by thermal energy alone without another energy source. A traditional battery-powered water meter has a power consumption of 36.3 µW which is much higher than 3.3 µW. Therefore, the device harvests ambient thermal energy to work, prolongs the life of the battery, and reduces the power cost. If

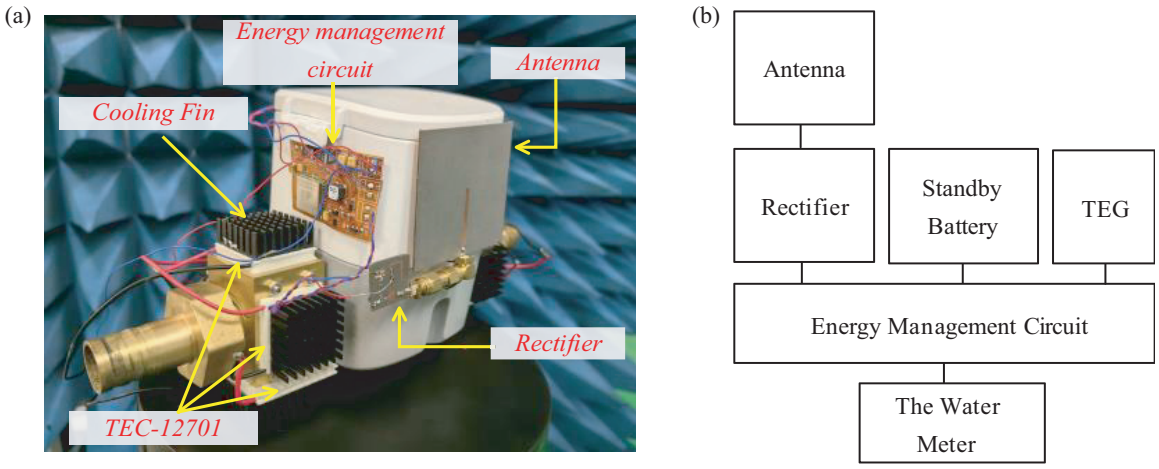

FIGURE 11. An electronic water meter with a coordinated ambient thermal and RF energy collection. (a) Fabricated water meter. (b) System block diagram.

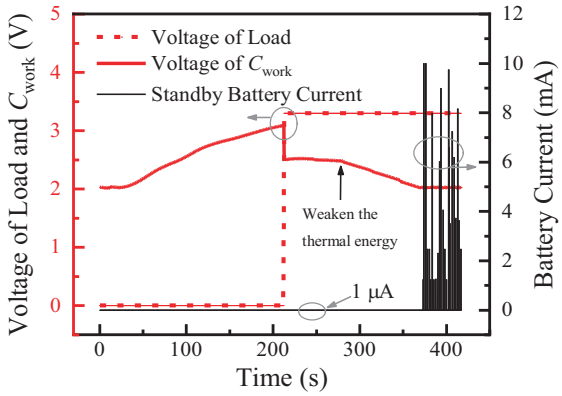

FIGURE 12. Power consumption testing of the device driven by TEGs.

we close the water valve switch to weaken the thermal energy so that the power from the TEG is insufficient, the water meter works with the power of the standby battery.

Using only a microwave source to drive the electronic water meter without TEGs is also tested in the microwave anechoic chamber which is already shown in Figure 8. The rectenna on the water meter converts RF power into DC power, and the energy management circuit will manage and store DC power in the same way as TEGs. The electronic water meter starts to operate until the voltage of C_{work} reaches 3.1 V, and it operates with RF power alone without the standby battery when the received power of the rectenna P_r reaches -2 dBm. Thus, both thermal and RF energy drives the water meter without the power of the battery successfully.

6. CONCLUSION

A hybrid energy harvesting circuit for ambient thermal and RF energy harvesting is proposed, including an antenna, a rectifier circuit, thermoelectric generators, and an energy management circuit. The $|S_{11}|$ of the proposed antenna in the WiFi band is below -20 dB. The measured efficiency of the rectifier exhibits 22% at -20 dBm input power, which is suitable for energy harvesting applications and gives a peak efficiency of 66% at 0 dBm at 2.45 GHz. Eight semiconductor plates TEC-12701 as the TEGs are attached to the surface of the water pipe to convert thermal energy into electrical energy. The FEH710 energy management circuit manages the energy from the rectifier and TEGs. The experiment results show that thermal and RF energy successfully drives the water meter. The circuit device significantly absorbs thermal and RF energy into electrical energy, reducing the dependence on conventional batteries. For further research, how to improve the conversion efficiency of rectenna in a low RF energy environment and how to reduce the power consumption of energy management circuits is a problem worthy of further study. In areas with RF energy coverage and temperature gradients, the proposed hybrid energy harvesting system drives not only smart water meters but also other low-power sensors such as temperature and humidity meters, and electricity monitoring meters. Therefore, the results of this study will also provide helpful inspiration and reference value for other energy harvesting and power supply applications.

ACKNOWLEDGEMENT

This work was supported in part by the National Science Foundation of China under Grant U22A2015 and 62071316. The

authors are with the School of Electronics and Information Engineering, Sichuan University, Chengdu 610064, China.

REFERENCES

[1] Halivni, B. and M. M. Peretz, "Current controlled transmitter for high frequency WPT utilizing non-invasive PCB integrated rogowski current sensor," in *2023 IEEE Applied Power Electronics Conference and Exposition (APEC)*, 1639–1644, IEEE, Orlando, FL, USA, Mar. 2023.

[2] Pandey, R., A. K. Shankhwar, and A. Singh, "An improved conversion efficiency of 1.975 to 4.744 GHz rectenna for wireless sensor applications," *Progress In Electromagnetics Research C*, Vol. 109, 217–225, 2021.

[3] Pandey, K. and R. Sadiwala, "Dual-port MIMO antenna design for IoT: Analysis and implementation," *Journal of Integrated Science and Technology*, Vol. 12, No. 3, 768, 2024.

[4] Salvati, R., V. Palazzi, G. Cicioni, G. Simoncini, F. Alimenti, M. M. Tentzeris, P. Mezzanotte, and L. Roselli, "Zero-power wireless pressure sensor based on backscatterer harmonic transponder in a WPT context," in *2022 Wireless Power Week (WPW)*, 199–202, IEEE, Bordeaux, France, Jul. 2022.

[5] Shiba, K. and M. Takahashi, "A development of WPT devices for wireless-powered small sensors for home health care," in *2022 International Symposium on Antennas and Propagation (ISAP)*, 81–82, IEEE, Sydney, Australia, 2022.

[6] He, Z. and C. Liu, "A compact high-efficiency broadband rectifier with a wide dynamic range of input power for energy harvesting," *IEEE Microwave and Wireless Components Letters*, Vol. 30, No. 4, 433–436, Apr. 2020.

[7] Pandey, R., A. K. Shankhwar, and A. Singh, "Design and analysis of rectenna at 2.42 GHz for Wi-Fi energy harvesting," *Progress In Electromagnetics Research C*, Vol. 117, 89–98, 2021.

[8] Lin, W. and R. W. Ziolkowski, "Wireless power transfer (WPT) enabled IoT sensors based on ultra-thin electrically small antennas," in *2021 15th European Conference on Antennas and Propagation (EuCAP)*, 1–4, IEEE, Mar. 2021.

[9] He, Z., J. Lan, and C. Liu, "Compact rectifiers with ultra-wide input power range based on nonlinear impedance characteristics of schottky diodes," *IEEE Transactions on Power Electronics*, Vol. 36, No. 7, 7407–7411, Jul. 2021.

[10] He, Z., H. Lin, and C. Liu, "A novel class-C rectifier with high efficiency for wireless power transmission," *IEEE Microwave and Wireless Components Letters*, Vol. 30, No. 12, 1197–1200, Dec. 2020.

[11] Takamori, R., M. Kawasaki, H. Seita, K. Nishimori, N. Honma, K. Nishikawa, Y. Maru, and S. Kawasaki, "Wireless sensor network in reusable vehicle rocket and low-power 20–30 GHz amplifier MMIC," in *2013 IEEE Wireless Power Transfer (WPT)*, 96–99, Perugia, Italy, May 2013.

[12] Jin, C., J. Wang, D. Y. Cheng, K. F. Cui, and M. Q. Li, "A novel wideband rectifier with two-level impedance matching network for ambient wireless energy harvesting," *Journal of Physics: Conference Series*, Vol. 1168, No. 2, 022020, Dec. 2019.

[13] Barton, T. W., J. M. Gordonson, and D. J. Perreault, "Transmission line resistance compression networks and applications to wireless power transfer," *IEEE Journal of Emerging and Selected Topics in Power Electronics*, Vol. 3, No. 1, 252–260, Mar. 2015.

[14] Boursianis, A. D., M. S. Papadopoulou, S. Koulouridis, P. Rocca, A. Georgiadis, M. M. Tentzeris, and S. K. Goudos, "Triple-band single-layer rectenna for outdoor RF energy harvesting applications," *Sensors*, Vol. 21, No. 10, 3460, May 2021.

[15] Kyono, T., R. O. Suzuki, and K. Ono, "Conversion of unused heat energy to electricity by means of thermoelectric generation in condenser," *IEEE Transactions on Energy Conversion*, Vol. 18, No. 2, 330–334, Jun. 2003.

[16] Auckland, D. W., R. Shuttleworth, A. C. Luff, B. P. Axcell, and M. Rahman, "Design of a semiconductor thermoelectric generator for remote subsea wellheads," *IEE Proceedings — Electric Power Applications*, Vol. 142, No. 2, 65–70, Mar. 1995.

[17] Kim, R.-Y. and J.-S. Lai, "A seamless mode transfer maximum power point tracking controller for thermoelectric generator applications," in *2007 IEEE Industry Applications Annual Meeting*, 977–984, IEEE, Sep. 2007.

[18] Collado, A. and A. Georgiadis, "Conformal hybrid solar and electromagnetic (EM) energy harvesting rectenna," *IEEE Transactions on Circuits and Systems I: Regular Papers*, Vol. 60, No. 8, 2225–2234, Aug. 2013.

[19] Lemey, S., F. Declercq, and H. Rogier, "Textile antennas as hybrid energy-harvesting platforms," *Proceedings of the IEEE*, Vol. 102, No. 11, 1833–1857, Nov. 2014.

[20] Guo, L., X. Gu, P. Chu, S. Hemour, and K. Wu, "Collaboratively harvesting ambient radiofrequency and thermal energy," *IEEE Transactions on Industrial Electronics*, Vol. 67, No. 5, 3736–3746, May 2020.

[21] Gu, X., L. Guo, M. Harouna, S. Hemour, and K. Wu, "Accurate analytical model for hybrid ambient thermal and RF energy harvester," in *2018 IEEE/MTT-S International Microwave Symposium — IMS*, 1122–1125, Philadelphia, PA, USA, Jun. 2018.

[22] Bakytbekov, A., T. Q. Nguyen, G. Zhang, M. S. Strano, K. N. Salama, and A. Shamim, "Dual-function triple-band heatsink antenna for ambient RF and thermal energy harvesting," *IEEE Open Journal of Antennas and Propagation*, Vol. 3, 263–273, 2022.

[23] Bakytbekov, A., Z. Iman, and A. Shamim, "3D printed bifunctional triple-band heatsink antenna for RF and thermal energy harvesting," in *2020 IEEE International Symposium on Antennas and Propagation and North American Radio Science Meeting*, 1563–1564, Montreal, QC, Canada, Jul. 2020.

[24] Jing, J., J. Pang, H. Lin, Z. Qiu, and C. Liu, "A multiband compact low-profile planar antenna based on multiple resonant stubs," *Progress In Electromagnetics Research Letters*, Vol. 94, 1–7, 2020.

[25] Liu, C., F. Tan, H. Zhang, and Q. He, "A novel single-diode microwave rectifier with a series band-stop structure," *IEEE Transactions on Microwave Theory and Techniques*, Vol. 65, No. 2, 600–606, Feb. 2017.

[26] Mahan, G., B. Sales, and J. Sharp, "Thermoelectric materials: New approaches to an old problem," *Physics Today*, Vol. 50, No. 3, 42–47, Mar. 1997.

[27] Song, C., P. Lu, and S. Shen, "Highly efficient omnidirectional integrated multiband wireless energy harvesters for compact sensor nodes of internet-of-things," *IEEE Transactions on Industrial Electronics*, Vol. 68, No. 9, 8128–8140, Sep. 2021.

[28] Vital, D., S. Bhardwaj, and J. L. Volakis, "Textile-based large area RF-power harvesting system for wearable applications," *IEEE Transactions on Antennas and Propagation*, Vol. 68, No. 3, 2323–2331, Mar. 2020.

[29] Sun, H., J. Huang, and Y. Wang, "An omnidirectional rectenna array with an enhanced RF power distributing strategy for RF energy harvesting," *IEEE Transactions on Antennas and Propagation*, Vol. 70, No. 6, 4931–4936, Jun. 2022.